Development of cobalt encased in nitrogen and sulfur co-doped carbon nanotube for non-precious metal catalyst toward oxygen reduction reaction

Tae-Hyun Kim[a], Byoung-In Sang[a] and Sung-Chul Yi[a,b,*]

[a]Department of Chemical Engineering, Hanyang University, Haengdang-dong, Seongdong-gu, Seoul 133-791, Korea
[b]Department of Hydrogen and Fuel Cell Technology, Hanyang University, Haengdang-dong, Seongdong-gu, Seoul 133-791, Korea

In this paper, cobalt embedded in nitrogen and sulfur co-doped carbon nanotubes (CoNSTs) were synthesized for oxygen reduction reaction (ORR) catalysts. The CoNSTs were prepared through a facile heat treatment method without any templates. Different amounts of the metal salt were employed to examine the physicochemical and electrochemical properties of the CoNSTs. The CoNSTs showed the bamboo-like tube morphology with the encased Co nanoparticles in the tubes. Through the x-ray photoelectron spectroscopy analysis, the catalysts exhibited different chemical states of the nitrogen and sulfur species. As a result, the CoNST performed high activity toward the ORR in an acidic condition with the onset potential of 0.863 V (vs. reversible hydrogen electrode). It was clearly demonstrated from the electrochemical characterizations that the quality of the nitrogen and sulfur species significantly influences the ORR activity rather than the total amount of the dopants.

Key words: Oxygen reduction reaction, Non-precious metal catalyst, Heteroatom doping, Carbon nanotube, Cobalt.

Introduction

A proton exchange membrane fuel cell (PEMFC) has attracted attention as one of the promising candidates to alternate the fossil-fueled engines. For the successful commercialization of the PEMFC, the activity of cathode catalyst toward oxygen reduction reaction (ORR) should be enhanced because of its sluggish kinetics. Although Pt-based catalysts have been widely employed for the ORR due to its highly efficient ORR activity, the expensive and scarce Pt still limit the commercialization of the PEMFC [1-3]. Hence, the development of an alternative catalyst with high ORR activity is necessary to replace the Pt-based catalyst.

For decades, researchers have intensively investigated on non-precious metal catalysts (NPMCs) in order to eliminate the Pt-based catalysts [4-18]. Among them, highly graphitized heteroatom (e.g., N, B, S, etc.) doped carbons through a high-temperature procedure with the transition metals (e.g., Fe, Co, Ni) have presented high ORR activity [4,5]. The dopants in the carbon matrix redistribute the spin and charge density on the neighboring carbon, resulting in the active sites for the ORR [6]. Furthermore, several researchers argued that the additional doping of heteroatoms in the N-doped carbon can further enhance the activity [7-11]. The additional doping can improve the physical and electronic characteristics of the doped carbon, hence

enhancing the ORR activity [12]. Currently, various nanostructures of the doped carbons have been shown as multi-layered graphene, onion-like carbon, and tubes. The morphology of the NPMC can be differed by the precursors and synthesis procedures [13-15]. There are several researches on the N-doped carbon nanotube (CNT) encasing the transition metal particles. They suggested that the embedded metal nanoparticles were favorable in activating the outer graphitic layers and thereby improve the active site density toward the ORR kinetics [16-18]. Despite the potential of the metal encapsulated in N-doped CNTs for the ORR catalysts, there are few investigations on the metal-encased dual heteroatoms co-doped CNTs for the NPMCs.

In this paper, cobalt embedded in nitrogen and sulfur co-doped CNTs were synthesized with a simple procedure without any templates. All catalysts showed the multi-walled and bamboo-shaped tubes within the Co nanoparticles. The CoNSTs were prepared with various ratios of the dopant precursors and the metal salt and characterized the physicochemical and electrochemical properties. From the electrochemical performances, the ORR activities of the CoNSTs were significantly influenced by the dopant contents of the nitrogen and sulfur species rather than the total amount of the dopants.

Experimental

Catalyst preparation

Dicyandiamide (DCDA), diphenyl disulfide (DDS),

*Corresponding author:
Tel : +82-2-2220-0481
Fax: +82-2-2298-5147
E-mail: scyi@hanyang.ac.kr

and cobalt (II) acetate hexahydrate (CoAc) were obtained from Sigma Aldrich. Typically, 1 g of DCDA, 0.5 g of DDS, and a predetermined amount of CoAc were dissolved in 150 ml of ethanol. Herein, 0.5 g, 0.25 g, and 0.125 g of CoAc were employed and denoted as the CoNST1, CoNST2, and CoNST3, respectively. The solution was dried in a convection oven at 60 $^{\circ}$C for overnight to evaporate ethanol. After evaporating solvent, the sample was ground with mortar and put in an alumina boat. The boat was put in tube furnace (DTF-50300, Deaheung Company) and the temperature was ramped to 900 $^{\circ}$C for 2 hrs under Ar atmosphere. After cooling down to room temperature, the heat-treated sample was dispersed in 1.0 M sulfuric acid at 80 $^{\circ}$C for 15 hrs to remove the unstable Co particles. After then, copious amount of distilled water was used to wash the acid-leached catalyst until the filtrate reaches neutral and dried in the oven for overnight. Finally, a second heat treatment was performed at 900 $^{\circ}$C for 2 hrs to eliminate the oxygen functional groups.

Characterizations

In order to characterize the nanostructures of the CoNSTs, field-emission scanning electron microscopy (SEM, Hitachi) and transmission electron microscopy (TEM, JEM 2100F, Jeol) experiment was carried out. X-ray photoelectron spectroscopy (XPS) was performed by using the Theta probe base system (Thermo Fisher Scientific Co.) equipped with an Al kα X-ray source to characterize the chemical states of the CoNSTs.

Rotating disk electrode experiment was performed to evaluate electrochemical properties of the catalysts in a three-electrode electrochemical cell with a potentiostat/galvanostat workstation (Gamry Reference 3000). Glassy carbon electrode (0.196 cm^2 area), Pt wire, and Ag/AgCl (3 M NaCl) were used for working, counter, and reference electrode, respectively. 5 mg of the catalysts and 5 μl of 5 wt% Nafion dispersion were dispersed in 2.5 ml of the mixed solvent (ethanol:DI water = 3:1(v/v)). After homogenization, the ink was drop-cast onto the glassy carbon electrode until the

catalyst loading reaches 600 μg cm^{-2}. The catalyst-coated glassy carbon electrode was electrochemically cleaned by the potential cycling from 0 to 1.2 V for 50 cycles in the N_2 saturated 0.1 M $HClO_4$ electrolyte with scan rate of 100 mV s^{-1} at room temperature. The cyclic voltammetry (CV) was conducted between 0 and 1.0 V with 50 mV s^{-1} scan rate. For the ORR measurements, linear sweep voltammetry (LSV) was carried out in the O_2-saturated electrolyte with the scan rate of 20 mV s^{-1} and a rotation rate of 1600 rpm.

Results and Discussion

Physicochemical characterizations

Fig. 1 exhibits the SEM and TEM images of the CoNSTs. As shown in Fig. 1(a-c), the catalysts presented the CNT morphology encasing the Co particles in the tip of the tube. The CoNSTs showed the length of several micrometers with the diameters ranging from 50 to 330 nm. According to previous reports, the CNT is formed based on the chemical interaction between π electrons of graphite and 3d-electrons of transition metals [17]. Hence, the Co nanoparticles are expected to form by the reduction of metal salt and initiate the CNT growth. It is clearly observed from Fig. 1(d-i) that the bamboo-like CNT encapsulated the Co nanoparticles, indicating the tip-growth mechanism. As shown in Figure 1e, g, and i, the Co particle presented the lattice distance of 0.21 nm, demonstrating the (111) plane of the metallic Co. In addition, the CoNSTs exhibited the multi-walled CNT with the interplanar spacing of 0.34 nm, corresponding to the (002) crystal plane of the graphitic carbon. Owing to the highly-graphitized carbon structure, the embedded Co particles were preserved after the harsh acid leaching process.

Fig. 2 shows the XPS spectra of the CoNSTs. As observed in Figs. 2(a, d, and g), the N 1s spectra were deconvoluted into three different nitrogen species at approximately 398.6, 401.0, and 403.4 eV, indicating to the pyridinic N, graphitic N, and oxidized N, respectively [18]. The S 2p spectra in Fig. 2 (b, e, and
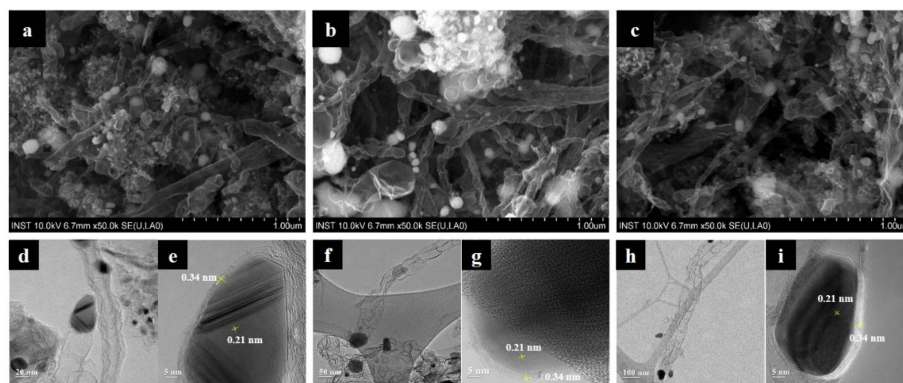

Fig. 1. SEM (a-c) and TEM (d-i) images of the CoNST1 (a,d,e), CoNST2 (b,f,g), and CoNST3 (c,h,i).

Table 1. Summary of the XPS spectra of the CoNSTs.

Sample	CoNST1	CoNST2	CoNST3
Total N [at.%]	6.23	3.62	3.92
Pyr-N [%][a]	43.35	25.73	33.01
Gr-N [%][a]	48.38	59.18	55.75
Ox-N [%][a]	8.27	15.09	11.24
Pyr-N/Gr-N	0.896	0.435	0.592
Total S [at.%]	1.58	1.01	0.76
C-S-C [%][b]	62.48	81.94	59.16
S_x^{n-} [%][b]	14.8	13.63	29.82
C-SO$_x$ [%][b]	22.71	4.43	11.02

a: Relative N species contents with respect to total N.
b: Relative N species contents with respect to total N.

h) showed four different sulfur species. The contribution at low binding energy at approximately 162 eV may be assigned to the Co-S and/or S = C-N bonds [19,20]. The peaks at approximately 163.5 and 164.9 eV demonstrate thiophene-like C-S-C structure, while the peak at approximately 167.9 eV suggests oxidized sulfur type (C-SO$_x$) [19]. From Fig. 2 (c, f, and i), the Co 2p spectra exhibited the core-level signals at approximately 780 eV and 796 eV, indicating the Co 2p$_{2/3}$ and Co 2p$_{1/2}$, respectively. The Co 2p spectra were deconvoluted into three different cobalt species as the metallic Co, Co^{2+}, and Co^{3+} at approximately 778.5, 780.2, and 781.5, respectively.

Although the CoNSTs showed the metallic Co particles from Fig. 1, the oxidized Co species may be corresponded to the surface oxidation and/or vulcanization of the metallic Co [20]. The details of the XPS spectra from Fig. 2 are tabulated in Table 1. The doped amount of the nitrogen species in the CoNSTs were 6.23, 3.62, and 3.92 at.% for the CoNST1, CoNST2, and CoNST3, respectively. Previously, there are reports that the n-type nitrogen in the carbon can improve the ORR activity by developing the disordered carbon nanostructures and altering the electronic structures of the carbon planes [6]. Particularly, the pyridinic N can be obtained by doping at the edge of the graphite planes and contribute one p-electron to the graphitic π system [10]. On the other hand, the graphitic N can be observed by doping within a graphene plane and contributes two p-electrons [21]. Although the pyridinic N is essential for creating the active sites toward the ORR, the graphitic N is also important to enhance the ORR activity through the modification of the electron distribution of carbon planes [14, 17, 21]. Hence, the ratio of the pyridinic N to graphitic N (Pyr-N/Gr-N) was further evaluated in Table 1. The ratios of the Pyr-N/Gr-N were 0.896, 0.435, and 0.592 for the CoNST1, CoNST2, and CoNST3, respectively. As tabulated in Table 1, the CoNST3 presented the highest S_x^{n-} content compared to the CoNST1 and CoNST2. It has been reported that the C-S-C enhance the ORR activity while the C-SO$_x$
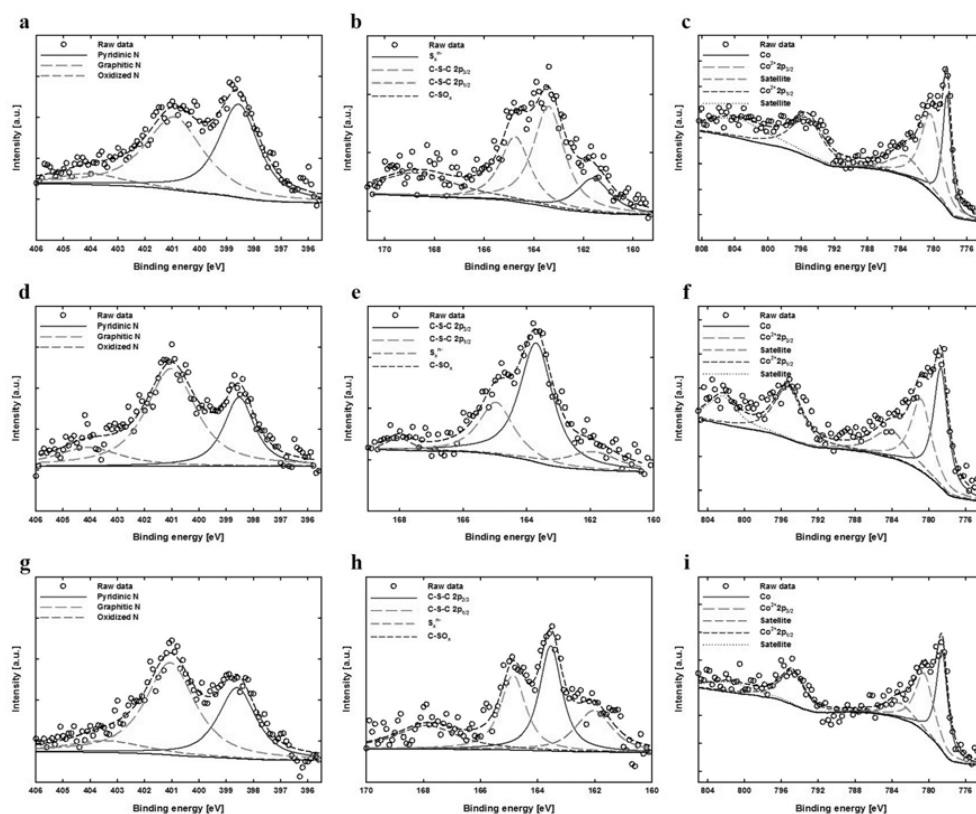

Fig. 2. XPS spectra of the N 1s (a, d, g), S 2p (b, e, h), and Co 2p (c, f, i). CoNST1 (a, b, c), CoNST2 (d, e, f), and CoNST3 (g, h, i).
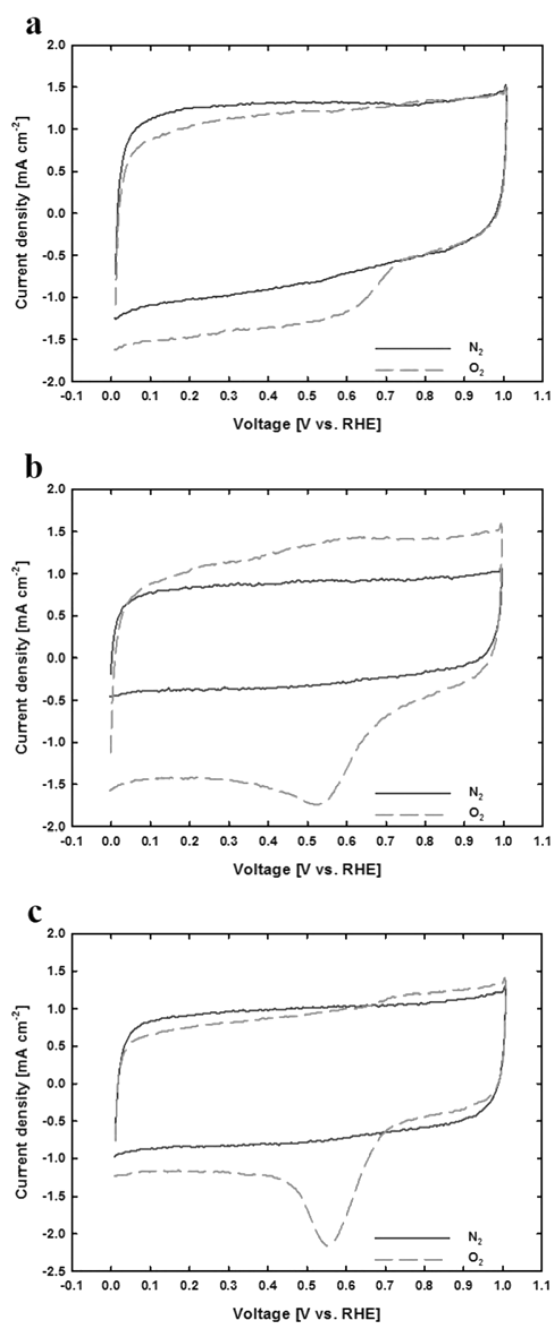
Fig. 4. ORR polarizations of the CoNSTs.

Fig. 3. CV curves of the CoNST1 (a), CoNST2 (b), and CoNST3 (c).

deteriorates the ORR activity [9, 10]. Recently, there are reports that the S_x^{n-} can also improve the activity toward the ORR [19, 20]. Hence, the electrochemical properties were further examined to elucidate the relationship between the chemical states and the electrochemical properties.

Electrochemical characterizations

Fig. 3 shows the CV profiles of the CoNSTs obtained in the 0.1 M $HClO_4$ electrolyte at room temperature. From the CV in the N_2-saturated electrolyte, an electrochemically accessible surface area (S_a) can be
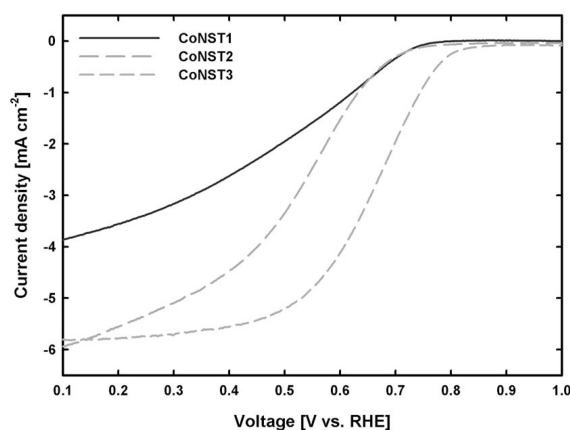
evaluated in order to characterize the surface area available for the ORR kinetics. The upper branch of CV between 0.3 V and 0.8 V corresponds to the pseudo capacitance associated with the electrolyte-accessible surface area. Thus, the S_a (m^2 g^{-1}) can be obtained from gravimetric double layer capacitance (C) (F g^{-1}):

$$C = \frac{I}{vm} \tag{4-1}$$

$$S_a = \frac{C}{C_{GC}} \tag{4-2}$$

where I indicates the current, v is the scan rate, m is the catalyst mass on the glassy carbon, and the C_{GC} is the double layer capacitance of the glassy carbon electrode (0.2 F m^{-2}). The CoNST3 showed the highest S_a value with 246.1 m^2 g^{-1}, compared to the CoNST1 (213.1 m^2 g^{-1}) and CoNST2 (177.9 m^2 g^{-1}). Because of the large S_a for the CoNST3, it presented the most positively-shifted peak at approximately 0.630 V in the O_2-saturated condition.

Fig. 4 shows the ORR polarizations of the CoNSTs at the rotation rate of 1600 rpm. As observed in Fig. 4, the ORR activity of the CoNST3 was superior to the other catalysts with the highest onset and half-wave potential. Furthermore, the diffusion-limited plateau is well-defined for the CoNST3, demonstrating the evenly-distributed active sites toward the ORR kinetics. Despite the highest doped amount of the nitrogen and sulfur species for the CoNST1, it exhibited the lowest ORR activity. It can be deduced that the ORR activity significantly depends on the types of the dopant species rather than the total dopant contents. Previous density functional theory (DFT) modeling suggested that the intermediates (e.g., *OO and *OOH) are favorable to adsorb on the graphitic sites rather than the edge sites [22, 23]. Thereby, the optimal ratio of the Pry-N/Gr-N is important for enhancing the ORR activity. On the other hand, the CoNST2 presented the lowest content of C-SO_x, while the CoNST3 showed the highest

amount of the S_x^{n-}. Although both the C-S-C and S_x^{n-} facilitate the ORR kinetics, it has been demonstrated by the DFT calculation and experimental that the S_x^{n-} significantly affects the activity by enhancing the selectivity of O_2 electro-reduction to H_2O [19]. Hence, the CoNST3 showed the enhanced ORR activity compared to the CoNST2 owing to the highest amount of the S_x^{n-} content. From the chemical states and the electrochemical properties of the CoNSTs, it can be concluded that the optimum Pry-N/Gr-N ratio and the S_x^{n-} content significantly affects the activity of the N, S co-doped carbon catalyst toward the ORR.

Conclusions

This paper reports on the electrochemical performances of cobalt-encapsulated in dual heteroatoms co-doped CNTs regarding the chemical states of the catalysts. Through the simple pyrolysis method, the CoNSTs showed the Co nanoparticle encased in the bamboo-like CNT. From the XPS analysis, various chemical states of the CoNSTs were observed by employing different amounts of the metal salts. As a result, the CoNST3 showed the highest ORR performance compared to the other catalysts. The CoNST3 demonstrated the evenly-distributed active sites toward the ORR with the large S_a. In addition, the optimal ratio of the pyridinic N to graphitic N and high content of the S_x^{n-} improved the ORR activity for the CoNST3. It is clearly demonstrated that the optimum ratio of the Pyr-N/Gr-N and S_x^{n-} significantly affected the ORR performance. Therefore, precise control of the doping heteroatoms in the carbon matrix is essential for enhancing the ORR activity of the NPMC.

Acknowledgments

References

1. B.C.H. Steele and A. Heinzel. Nature 414[6861] (2001) 345-352.
2. C.M. Sánchez-Sánchez, and A.J. Bard. Anal. Chem. 81[19] (2009) 8094-8100.
3. Y. Bing, H. Liu, L. Zhang, D. Ghosh, and J. Zhang. Chem. Soc. Rev. 39[6] (2010) 2184-2202.
4. G. Wu, K.L. More, C.M. Johnston, and P. Zelenay. Science 332[6028] (2011) 443-447.
5. C.H. Choi, S.H. Park, and S.I. Woo. Appl. Catal. B Environ. 119-120 [30] (2012) 123-131.
6. Z. Zhao, M. Li, L. Zhan, L. Dai, and Z. Xia. Adv. Mater. 27[43] (2015) 6834-6840.
7. J. Liang, Y. Jiao, M. Jaroniec, and S.Z. Qiao. Angew. Chem. Int. Ed. 51[46] (2012) 11496-11500.
8. C.H. Choi, S.H. Park, and S.I. Woo. ACS Nano 6[8] (2012) 7084-7091.
9. C.H. Choi, M.W. Chung, Y.J. Jun, and S.I. Woo. RSC Adv. 3[30] (2013) 12417-12422.
10. J. Shi, X. Zhou, P. Xu, J. Qiao, Z. Chen, and Y. Liu. Electrochim. Acta. 145[1] (2014) 259-269.
11. K. Hu, L. Tao, D. Liu, J. Huo, and S. Wang. ACS Appl. Mater. Interfaces 8[30] (2016) 19379-19385.
12. Z. Zhao and Z. Xia. ACS Catal. 6[3] (2016) 1553-1558.
13. Y. Tang, B.L. Allen, D.R. Kauffman, and A. Star. J. Am. Chem. Soc. 131[37] (2009) 13200-13201.
14. G. Wu, M. Nelson, S. Ma, H. Meng, G. Cui, and P.K. Shen. Carbon 49[12] (2011) 3972-3982.
15. Z. Wen, S. Ci, F. Zhang, X. Feng, S. Cui, S. Mao, S. Luo, Z. He, and J. Chen. Adv. Mater. 24[11] (2012) 1399-1404.
16. S. Fu, C. Zhu, H. Li, D. Du, and Y. Lin. J. Mater. Chem. A 3[24] (2015) 12718-12722.
17. X. Wang, Q. Li, H. Pan, Y. Lin, Y. Ke, H. Sheng, M.T. Swihart, and G. Wu. Nanoscale 7[47] (2015) 20290-20298.
18. T.H. Kim, C.Y. Jung, R. Bose, and S.C. Yi. Carbon 139 (2018) 656-665.
19. J. Zhu, K. Li, M. Xiao, C. Liu, Z. Wu, J. Ge, and W. Xing. J. Mater. Chem. A 4[19] (2016) 7422-7429.
20. Z. Wang, S. Peng, Y. Hu, L. Li, T. Yan, G. Yang, D. Ji, M. Srinivasan, Z. Pan, and S. Ramakrishna. J. Mater. Chem. A 5[10] (2017) 4949-4961.
21. Q. Li, R. Cao, J. Cho, and G. Wu. Adv. Energy Mater. 4[6] (2014) 1301415-1301433.
22. R.A. Sidik, A.B. Anderson, N.P. Subramanian, S.P. Kumaraguru, and B.N. Popov. J. Phys. Chem. B 110[4] (2006) 1787-1793.
23. F. Studt. Catal. Lett. 143[1] (2013) 58-60.